Contents lists available at ScienceDirect

Food and Bioproducts Processing

journal homepage: www.elsevier.com/locate/fbp

Multiphysics modeling of convective cooling of non-spherical, multi-material fruit to unveil its quality evolution throughout the cold chain

G. Tagliavini[a,b], T. Defraeye[a,*], J. Carmeliet[b]

[a] Empa, Swiss Federal Laboratories for Materials Science and Technology, Laboratory for Biomimetic Membranes and Textiles, Lerchenfeldstrasse 5, CH-9014 St. Gallen, Switzerland
[b] Chair of Building Physics, ETH Zurich, Stefano-Franscini-Platz 1, 8093 Zürich, Switzerland

ARTICLE INFO

Article history:
Received 5 April 2019
Received in revised form 5 July 2019
Accepted 23 July 2019
Available online 30 July 2019

Keywords:
Fruit cooling
Computational fluid dynamics
Cold chain
Quality prediction
Mangos
Digital twin

ABSTRACT

Convective cooling is essential in many supply chain unit operations for refrigerated transport and cold storage of fresh products. Fruit must be kept at low temperatures to preserve quality and to slow down biochemically-driven food degradation. Along the cold chain, heterogeneities in temperatures are present among individual products, which influence the resulting product quality, causing significant food losses. This study presents a thermo-fluid dynamic model of a single mango fruit to better understand the convective cooling behavior of fruits with more complex, non-spherical shapes and a heterogeneous composition. To explain the biochemical and biological processes affecting the product's final quality, experimental data from the literature are used to calibrate kinetic rate laws for the prediction of different quality attributes (overall quality, flesh firmness, titratable acidity, total soluble solids and vitamin content) over time.

The accuracy of airflow modeling and of applying a realistic fruit shape are assessed. It is quantified how much higher airspeeds lead to faster cooling of the pulp and seed, and how strong non-uniform temperature heterogeneities are inside the fruit. From sensitivity analysis, air temperature has the most impact on fruit temperature during cooling, while thermal properties and fruit size have a minor influence. The evolution of the quality attributes is shown at different temperatures, and the heterogeneities in quality within the mango fruit are also investigated. The obtained insights will help advance cooling process optimization for other complex-shaped, multi-material fruit and vegetables.

1. Introduction

Fresh fruits and vegetables need to be cooled down soon after harvest to preserve their quality and maximize shelf life. The reason is that temperature is the single most important environmental parameter affecting the physiological degradation processes of the product. These processes are slowed down at low temperatures. As such, fast and uniform cooling of the fruit after harvest is essential. To this end, forced-convective airflow cooling is used as a key unit operation in food supply chains. However, during convective cooling, the products are stacked in large assemblies, namely in ventilated packaging, such as carton boxes. Significant heterogeneities in cooling behavior and therefore in resulting quality, have been found between individual products (Defraeye et al., 2013a; O'Sullivan et al., 2016; Wu and Defraeye, 2018). These non-uniformities are induced by the complex turbulent flow field, caused by the package design with vent holes at a specific location, but also by the heating up of the air that passes over subsequent fruit (Defraeye et al., 2014; Han et al., 2015). A typical example of an important fruit for the postharvest cold chain is mango fruit. From 2012 to 2016, the consumption of mangos (*Mangifera*

* Corresponding author.
E-mail address: thijs.defraeye@empa.ch (T. Defraeye).
https://doi.org/10.1016/j.fbp.2019.07.013

indica) increased up to 288,000 t, in Europe (CBI – Ministry of Foreign Affairs, 2016). Like other tropical fruits, mangos are very susceptible to the cooling conditions and storage temperature. These non-spherical fruits are composed of pulp and seed with different thermal properties and thereby present a complex cooling behavior.

Much research has been undertaken on identifying the heterogeneities in cooling and fruit quality evolution between individual products in large assemblies (O'Sullivan et al., 2016; Zou et al., 2006). However, the corresponding heterogeneities within a product are often not focused on. The main reason is that most fresh products are spherical or cylindrical and have quite uniform thermal properties, by which cooling can be approximated with simple analytical models. For fruits with a more complex geometrical shape and composition, such as mangos, the convective cooling process and associated quality evolution within the fruit is driven by the surrounding turbulent flow field and is much less understood. Such knowledge is essential to improve the cooling of such non-spherical fruits with a composite structure in order to reduce food losses.

To gain a deeper knowledge of the cooling of fresh products, two main approaches are used: numerical simulations, often involving computational fluid dynamics (CFD), and experimental studies. Numerical models focus on heat transfer (Alvarez and Flick, 1999b; Beukema et al., 1982) and investigate, among others, the influence of air speed, turbulence and surface roughness on fruit cooling (Alvarez and Flick, 1999a; Raval et al., 2013; Redding et al., 2016). Often, CFD simulations are carried out using discretely modeled spherical fruits and homogeneous thermal properties (Alvarez et al., 2003; Defraeye et al., 2012), or a porous media approach (Delele et al., 2013; Zou et al., 2006), to model stacked products for package design and optimization (Dehghannya et al., 2011; Defraeye et al., 2014, 2015). Only a few studies have used ellipsoidal fruit shapes (O'Sullivan et al., 2016; Saudreau et al., 2007). In all these studies, the focus is always on cooling rates and heterogeneities in temperatures while the impacts of non-uniform intraproduct cooling on biochemical and biological processes, so on the quality attributes, are neglected.

Likewise, many experimental studies have investigated the shelf life and evolution of various quality attributes (e.g., firmness, sugar content, titratable acidity, vitamin content) under different cooling conditions (Baloch et al., 2011; Noiwan et al., 2017; Nunes et al., 2006), but these studies did not directly link the results to the thermal heterogeneities within the products.

To tackle these knowledge gaps, the objective of this study is to gain a better insight into how heat-sensitive products with a complex, non-spherical shape and heterogeneous composition behave under convective cooling. For this purpose, a computational model for fruit cooling is developed, in which the evolution of several quality attributes (such as firmness, sugar content, acidity, vitamin content) is included, by modeling the biochemical reactions rates. By linking physical and biochemical processes, we quantify the evolution of multiple quality attributes and remaining quality over time. The model represents a non-spherical product composed of two different materials, pulp and seed, with different thermal properties. First, the accuracy of airflow modeling and of applying a realistic fruit shape are appraised. Then, it is quantified how much higher airspeeds lead to faster cooling of the fruit, and how strong non-uniform temperature heterogeneities are inside of it. Next, a sensitivity analysis is performed to evaluate the impact of various input parameters, namely, air speed, air temperature, flow turbulence, thermal properties and geometry, on product cooling. Then, to describe the quality attributes mentioned above, kinetic rate laws representing biochemical reactions are calibrated with experimental data and included in the model.

The work presented in this paper can be used as building block for a so-called digital twin (Defraeye et al., 2019), a virtual representation of the real fruit and is able to capture the kinetics related to cooling and biochemical response throughout the cold chain. Mangos are transported in ventilated packages in which high temperature heterogeneities among fruits are present. Temperature sensors can be placed inside these packages to monitor the air temperature in the proximity of each fruit. These temperature data can serve as initial conditions for the single fruit model and, in this way, it will be able to mimic the real fruit behavior and evaluate quality losses along the cold chain at different environmental conditions. Thanks to such a fruit model with explicit airflow modeling, we are able to gain insights in how mango fruit cools down and what the remaining quality attributes are, such as firmness and vitamin content.

2. Materials and methods

2.1. *Numerical model*

The computational model takes into consideration both the solid (fruit) and the fluid (air) domains, so a conjugate approach is used. An ellipsoid is used to represent the mango fruit. To account for both the fruit pulp and seed, an inner, smaller ellipsoid is created, inside that of the fruit. Based on symmetry, the domain size is reduced by a factor of 2 along the axis of symmetry. The major and minor semi-axes are, respectively, 0.075 m (b) and 0.046 m (a) long for the mango fruit, and $0.45b$ and $0.45a$ for the seed. The complete model geometry is shown in Fig. 1. The domain sizes and grid density are based on best practice guidelines and a grid sensitivity analysis (Franke et al., 2007; Roache, 1994).

The grid consists of 1.45×10^5 and 2.22×10^4 elements for the air and solid domain, respectively, as detailed in Fig. 2. On the surface of the external ellipsoid, a boundary-layer mesh is created, and the thickness of the first layer is chosen to obtain a $y^+ \sim 1$ in the wall-adjacent cell. On the prismatic cells of the boundary layer, tetrahedral cells are placed with a progressively increasing size (growth factor of 1.1) from the fruit wall to the flow domain, and with a maximum size of 2×10^{-3} m. These cells are confined inside a rectangle placed around the outer ellipsoid (see Fig. 2), with the following dimensions: $6b$ height and $3b$ width. Outside this rectangle, the cells are still tetrahedral but with larger size (maximum of 4.2×10^{-2} m), except for the inlet and outlet regions, for which a fixed number of elements is used as a refinement criterion (100 elements). The spatial discretization error was estimated by means of Richardson extrapolation (Roache, 1994), considering five different grids with a refinement factor of 0.7. This error is 1.64% for the convective heat transfer coefficient (CHTC) ($W\,m^{-2}\,K^{-1}$), 0.05% for shear stress (Pa) and 1.12% for wake length (m).

Concerning the airflow, at the domain inlet, a uniform speed U_{in}, is imposed (see Fig. 1). Five different air speeds (U_{in}) are evaluated in the range of 0.1–10 m/s with an increasing factor of $10^{0.5}$, namely, 0.10, 0.32, 1.0, 3.2 and 10 m/s. These values result in Reynolds numbers (Re) from 1.04×10^3 to 1.04×10^5

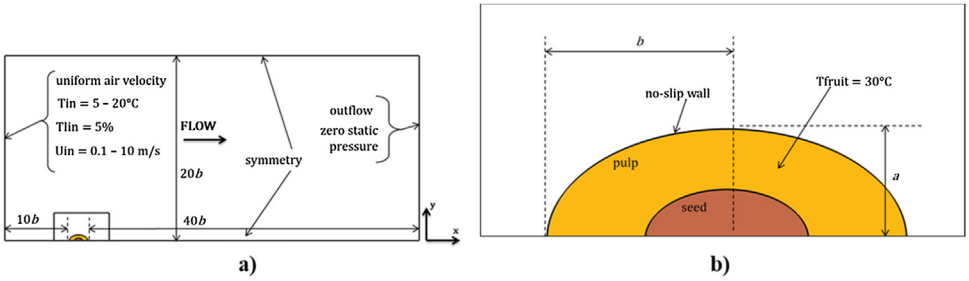

Fig. 1 – (a) Computational domain with dimensions and boundary conditions. (b) Detail of dimensions, boundary conditions and materials.

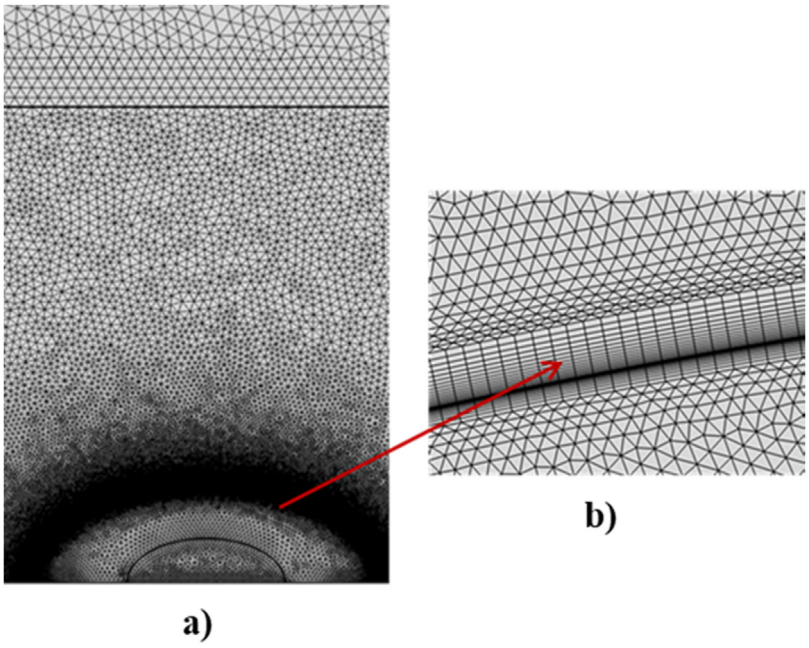

Fig. 2 – (a) Model computational grid: subdivision of the domain and different cell sizes. (b) Detail of the boundary-layer mesh.

(with $Re = U_{in}2b/\upsilon$), covering the speed range usually found in cold chain unit operations (Mercier et al., 2017; Zhao et al., 2016). At the outlet, a zero static pressure is established. A no-slip condition with zero roughness is set at the ellipsoid wall, and the symmetry boundary condition is selected for the lateral boundaries of the flow domain (Fig. 1). Following a comparison of different turbulence models (SST k–ω (Menter, 1994), k–ω (Wilcox, 1988), k–ε (Launder and Spalding, 1974) and Spalart-Allmaras (Spalart and Allmaras, 1992)), the k–ω shear stress transport (SST) is chosen to model the turbulence. A study on boundary-layer modeling of airflow around an apple fruit (spherical domain) by Defraeye et al. (2013b) shows that this model is the most suitable for accurate predictions of the onset and amount of flow separation under adverse pressure gradients. The SST k–ω model exploits the k–ω formulation in the inner parts of the boundary layer (viscous sublayer), such that it can be used as a low-Re turbulence model, without any extra damping functions. In the free-stream region, the SST k–ω model switches to k–ε behavior.

Regarding heat transfer, an initial uniform temperature of 30 °C (T_{fruit}) is set for the fruit domain, which is a typical temperature at harvest. Different air temperatures are imposed at the inlet, namely, 5, 8, 10, 12 and 20 °C. At the outlet and lateral boundaries, outflow and symmetry condition are chosen, respectively. Thermal properties of air are assigned, according to the values provided by the American Society of Heating, Refrigeration and Air-Conditioning Engineers (ASHRAE, 2001).

The main difficulties in evaluating thermal behavior of biological products, and thus quality evolution, reside in temperature heterogeneities (within the same box) and biological diversity (different cultivars). To accurately capture these variabilities, the thermal properties of the mango pulp and seed are independently expressed as a function of the chemical components and fruit temperature, according to ASHRAE (2006), in order to reproduce the real thermal behavior of the product as accurately as possible. The equations describing each property are listed below:

$$\rho_f = \sum_{i=1}^{n} X_i^v \rho_i \tag{1}$$

$$c_{p_f} = \sum_{i=1}^{n} X_i^m c_{p_i} \tag{2}$$

$$\lambda_f = \sum_{i=1}^{n} X_i^v \lambda_i \tag{3}$$

where X_i^v is the volume fraction, ρ_i is the density (kg m^{-3}), X_i^m is the mass fraction, c_{p_i} is the specific heat capacity (J kg^{-1} K^{-1}) and λ_i is the thermal conductivity (W m^{-1} K^{-1}) of the component i (see Table 1). In Eqs. (1)–(3), ρ_f (kg m^{-3}), c_{p_f} (J kg^{-1} K^{-1}) and λ_f (W m^{-1} K^{-1}) are the total density, the total specific heat

Table 1 – (a) Mass fractions of mango pulp and seed components and (b) thermal properties as a function of fruit temperature to characterize realistic thermal behavior (ASHRAE, 2006).

(a)

Mass fraction (%) of ripe mango pulp (ASHRAE, 2006)		
Components	Water	81.71
	Protein	0.51
	Fat	0.27
	Carbohydrates	17.00
	Fiber	1.80
	Ash	0.50
Mass fraction (%) of mango seed (Nzikou et al., 2010)		
Components	Water	45.20
	Protein	6.36
	Fat	13.00
	Carbohydrates	32.24
	Fiber	2.02
	Ash	3.20

(b)

Thermal properties of pulp components (ASHRAE, 2006)		
Specific heat capacity (J/(kg K))	Water	$c_p = 4.1289 - 9.0864 \times 10^{-3}T + 5.4731 \times 10^{-6}T^2$
	Protein	$c_p = 2.0082 + 1.2089 \times 10^{-3}T - 1.3129 \times 10^{-6}T^2$
	Fat	$c_p = 1.9842 + 1.4733 \times 10^{-3}T - 4.8008 \times 10^{-6}T^2$
	Carbohydrates	$c_p = 1.5488 + 1.9625 \times 10^{-3}T - 5.9399 \times 10^{-6}T^2$
	Fiber	$c_p = 1.8459 + 1.8306 \times 10^{-3}T - 4.6509 \times 10^{-6}T^2$
	Ash	$c_p = 1.0926 + 1.8896 \times 10^{-3}T - 3.6817 \times 10^{-6}T^2$
Density(kg/m^3)	Water	$\rho = 9.9718 \cdot 10^2 + 3.1439 \times 10^{-3}T - 3.7574 \times 10^{-3}T^2$
	Protein	$\rho = 1.3299 \times 10^3 - 5.1840 \times 10^{-1}T$
	Fat	$\rho = 9.2559 \times 10^2 - 4.1757 \times 10^{-1}T$
	Carbohydrates	$\rho = 1.5991 \times 10^3 - 3.1046 \times 10^{-1}T$
	Fiber	$\rho = 1.3115 \times 10^3 - 3.1046 \times 10^{-1}T$
	Ash	$\rho = 2.4238 \times 10^3 - 2.8063 \times 10^{-1}T$
Thermal conductivity (W/(m K))	Water	$\lambda = 5.7109 \times 10^{-1} + 1.7625 \times 10^{-3}T - 6.7036 \times 10^{-6}T^2$
	Protein	$\lambda = 1.7881 \times 10^{-1} + 1.1958 \times 10^{-3}T - 2.7178 \times 10^{-6}T^2$
	Fat	$\lambda = 1.8071 \times 10^{-1} - 2.7604 \times 10^{-3}T - 1.7749 \times 10^{-6}T^2$
	Carbohydrates	$\lambda = 2.0141 \times 10^{-1} + 1.3874 \times 10^{-3}T - 4.3312 \times 10^{-6}T^2$
	Fiber	$\lambda = 1.8331 \times 10^{-1} + 1.2497 \times 10^{-3}T - 3.1683 \times 10^{-6}T^2$
	Ash	$\lambda = 3.2962 \times 10^{-1} + 1.4011 \times 10^{-3}T - 2.9069 \times 10^{-6}T^2$

capacity and the total thermal conductivity, respectively. This approach allows an accurate reproduction of the fruit behavior during cooling and takes into account temperature heterogeneities, so that it is possible to describe the real behavior of the mango fruit according to its temperature history. In the presented study, the chosen values for all the different components are listed in Table 1, and they are representative for a mango fruit (ASHRAE, 2006; Nzikou et al., 2010).

2.2. *Governing equations*

Following the approach commonly used in forced-convective cooling studies (Han et al., 2015; Zhao et al., 2016), the Navier–Stokes equations are solved in a steady-state regime and, in a further step, the transient energy equations in both air and fruit are solved simultaneously, to obtain the temperature distribution profiles in the air and in the fruit, respectively. Given the high Reynolds numbers, forced-air convection is present, and so buoyancy is not modeled. The airflow around the mango is viewed as a steady, turbulent and incompressible flow of dry air. Therefore, the Reynolds-averaged Navier–Stokes (RANS) and continuity equations are expressed as:

$$\nabla \cdot \bar{\mathbf{u}} = 0 \tag{4}$$

$$\rho_a \bar{\mathbf{u}} \cdot \nabla \bar{\mathbf{u}} = -\nabla p + \nabla \cdot [\mu_a(\nabla \bar{\mathbf{u}} + (\nabla \bar{\mathbf{u}})^T - \rho_a \overline{\mathbf{u}'\mathbf{u}'})] + \bar{\mathbf{F}} \tag{5}$$

where $\bar{\mathbf{u}}$ is mean air velocity (m s^{-1}), ρ_a is the density of air (kg m^{-3}), p is the air pressure (Pa), μ_a is the dynamic viscosity of air (Pa s) and $\bar{\mathbf{F}}$ is the source term for the momentum equation. As mentioned above, the SST k–ω turbulence model is chosen to solve the RANS equations.

The temperature of the air and fruit, respectively, is time-dependent, so a transient energy equation is solved to evaluate the temperature field in the airflow:

$$\rho_a c_{p_a} \frac{\partial T_a}{\partial t} + \rho_a c_{p_a} \bar{\mathbf{u}} \cdot \nabla T_a = \nabla \cdot (\lambda_a \nabla T_a) \tag{6}$$

where c_{p_a} is the specific heat capacity of air (J kg^{-1} K^{-1}), λ_a is the thermal conductivity of air (W m^{-1} K^{-1}), T_a is the air temperature (K). At the same time, we need to solve the equation

describing the transient heat conduction in the fruit to obtain the temperature field inside the mango:

$$\rho_f c_{p_f} \frac{\partial T_f}{\partial t} = \nabla \cdot (\lambda_f \nabla T_f) \tag{7}$$

where ρ_f is the fruit density (kg m^{-3}), c_{p_f} is the fruit specific heat capacity (J kg^{-1} K^{-1}), λ_f is the thermal conductivity of the fruit (W m^{-1} K^{-1}) and T_f is the fruit temperature (K).

To account for the convective heat transfer, the conjugate heat transfer method is applied by setting the same physics (heat transfer) in both fluid and solid domain, so that the continuity of the thermal problem at the fruit–air interface is guaranteed. The local heat transfer coefficient does not need to be specified and can instead be derived afterwards directly from the computational solution. The continuity of temperatures and heat fluxes at the fruit surface is described by the following equations:

$$T_f(\mathbf{x}, t) = T_a(\mathbf{x}, t) \tag{8}$$

$$\boldsymbol{n} \cdot \lambda_f \nabla T_f(\mathbf{x}, t) = \boldsymbol{n} \cdot \lambda_a \nabla T_a(\mathbf{x}, t) \tag{9}$$

where $\mathbf{x}$ is the Cartesian coordinate and $\boldsymbol{n}$ is the normal vector at the fruit surface at the position $\mathbf{x}$.

2.3. Modeling the evolution of fruit quality

2.3.1. The kinetic rate law model for quality attributes

As mentioned in Section 1, chemical, biochemical and physical changes inside fruits and vegetables can affect different quality attributes. Among the most important attributes for mango quality, are overall quality, firmness, titratable acidity, vitamin and sugar content.

Fruit overall quality serves as a general indicator of the marketability of the mangos up to a threshold value of 10%, below which the product is not acceptable anymore by the consumer. Among the other attributes, firmness indicates the fruit hardness and is one of the main aspects used to define the ripening stage of a fruit. It can refer either to the fruit peel or its flesh, according to whether the measurements are performed with or without the peel. In this study, only flesh firmness is considered, since the peel is not included in the model. Sugar content is usually named total soluble solid content and represents the solids concentration of a sucrose-containing solution while titratable acidity is a measure of the amount of citric acid present in a solution in (g/kg) or (%). β-Carotene is a pigment from the vitamin family of carotenes, from which vitamin A can be extracted. Vitamin C, also known as ascorbic acid, is an essential nutrient.

The evolution of these attributes can be represented by kinetic rate laws (mathematical models) that includes temperatures, rate constants and activation energies. Such kinetic equations are usually provided for the description of biochemical reactions in food (Robertson, 1993; Van Boekel, 2008). A generic form can be written as:

$$-\frac{dA}{dt} = kA^n \tag{10}$$

where A is a quality attribute, t is the time (s), k is the rate constant (s^{-1}) and n is the order of the reaction. In this study, both zero- and first-order reactions, with positive or negative rate constants, are taken into account.

A zero-order reaction describes the change over time of the parameter A as a linear curve with k as slope. Therefore, Eq. (10) can be integrated for a constant value of k, obtaining the following expression:

$$A = A_0 - kt \tag{11}$$

in which A_0 is the value of parameter A at $t = 0$. For the first-order reaction, the integration of Eq. (10) for a constant value of k gives following expression:

$$A = A_0 \cdot e^{-kt} \tag{12}$$

Most of the biochemical processes that occur in the fruit during storage are strongly temperature-dependent. In this view, temperature dependency must be included in the kinetic rate law. To achieve this, the rate constant k is often described by an Arrhenius relationship (Robertson, 1993):

$$k(T) = k_0 \cdot e^{-E_a/RT} \tag{13}$$

where k_0 is a constant (s^{-1}), E_a is the activation energy (J mol^{-1}), R is the ideal gas constant (8.314 (J mol^{-1} K^{-1})) and T is the absolute temperature (K).

2.3.2. Calibration of the quality model

To model the evolution of different quality attributes, Eqs. (11) and (12), combined with Eq. (13), are fitted (at a constant temperature) to experimental data of flesh firmness, titratable acidity, soluble solid content, vitamin content and β-carotene from measurement found in literature and performed on mangos kept in cold rooms at different storage temperatures (Karithi, 2016). The correlation obtained from the fitting is included in the computational model. Given that A, A_0 and t are known, the reference value for k can be directly determined from Eqs. (11) or (12) at a chosen reference temperature, depending on the considered attribute. As a second step, the dependency of the rate constant on the temperature is introduced by the evaluation of the Q_{10} value, which is defined as:

$$Q_{10} = \frac{k_{T+10}}{k_T} \tag{14}$$

where k_{T+10} and k_T are the rate constants at temperature T and $T + 10$, respectively. The typical Q_{10} values for biochemical processes inside fruits fall between 2 and 3. Once the Q_{10} value is known, the activation energy (E_a) can easily be derived from the following equation:

$$E_a = \frac{R \ln(Q_{10})}{(1/T) - (1/(T + 10))} \tag{15}$$

Finally, k_0 can be evaluated, once k, Q_{10} and E_a are known. Then, all the values in Eq. (13) are known, and the final equation can be implemented in the model. The values of Q_{10} and E_a, together with R^2 from the fitting, are listed in Table 2.

2.4. Numerical simulations

The simulations are carried out in COMSOL Multiphysics 5.3a, which is based on the finite element method. In forced-air cooling, heat conduction occurs on the fruit surface, and heat convection moves the heat away from its surface to the surrounding airflow. General information on the numerical

Table 2 – Values from the calibration of kinetic rate law models with experimental data from Karithi (2016).

Quality attributes	Kinetic rate law models calibration values		
	Q_{10}	E_a (J/mol)	R^2
Overall quality	2.0	46858	0.94
Flesh firmness	3.0	74159	0.97
Total soluble solids	2.1	47953	0.99
Titratable acidity	2.1	49720	0.98
Vitamin C	2.1	49607	1.00
β-Carotene	2.4	59071	0.99

methods used to discretize and solve the transport equations in CFD can be found in Franke et al. (2007). As mentioned above, different turbulence models are tested and the SST k–ω turbulence model (Section 2.1) occurred to be the most accurate in predicting convective heat transfer. To validate the chosen model, averaged Nusselt numbers over the fruit surface from the simulations are compared with those found in the literature for flow around an ellipsoid (Clary and Nelson, 1970), as shown in Section 2.5.

To speed up the computation, a steady-state calculation is initially performed to solve the airflow around the fruit. Since the airflow is stationary, it does not need to be resolved during the transient calculation, so only the heat transfer is solved with a time-dependent simulation. The segregated solver is used to solve the airflow, and the fully coupled solver is applied to solve the heat transfer and quality model while for both calculations, namely, the PARADISO solver scheme (COMSOL, 2017). The time-dependent problem runs with an initial time step of 1 s, progressively increasing up to a time step of 1600 s, to account for 20 days of simulation, which is a typical duration for the cold chain of fresh mangos.

Another set of thermal simulations is performed, without solving for the fluid domain. This model is used for comparison purposes to tackle the importance of modeling the flow domain. In this simplified model, an averaged CHTC is imposed at the fruit surface and is taken from the Nusselt number equation for the flow around an ellipsoid at different Re (Clary and Nelson, 1970). A time-dependent calculation is done to solve the heat transfer problem.

2.5. *Turbulence model validation*

Before analyzing the cooling performance of the mango fruit, the accuracy of the CFD model is assessed by comparing results from different turbulence models, following the approach of Defraeye et al. (2013b). Different turbulence models (SST k–ω (Menter, 1994), k–ω (Wilcox, 1988), k–ε (Launder and Spalding, 1974) and Spalart–Allmaras (Spalart and Allmaras, 1992)) are tested and the values of the averaged Nusselt numbers over the fruit surface from each model are compared with values obtained from the following experimental relation described by Clary and Nelson (1970):

$$\overline{Nu} = 0.489\, Pr^{1/3} Re^{0.557} \left(\frac{b}{c}\right)^{-0.070} \left(\frac{a}{c}\right)^{-0.44} \tag{16}$$

in which Pr is the Prandtl number, Re is the Reynolds number, b is the major semi-axis (m), a is the minor semi-axis (m) and c is the semi-axis in the third dimension perpendicular to the major axis (in this study $c = a$). As shown in Fig. 3, the SST k–ω proves to be the most accurate among the ones tested, with a mean absolute error of 4%, whereas the others showed errors above 12% from the analytical values.

2.6. *Sensitivity analysis*

A sensitivity analysis is conducted to assess the influence of different model input parameters on the fruit temperature. To do so, the following input values are considered:

- inlet air temperature
- inlet air velocity
- turbulence intensity
- pulp thermal properties
- seed thermal properties
- major and minor semi-axis length

Since the most relevant aspect in this work is the cooling behavior of a single mango, the choice of the reference model output parameter used to quantify the impact of input parameters on the solution, by means of sensitivity analysis, is chosen to be the average temperature of the fruit. With this in mind, the relative sensitivities are calculated as normalized partial derivatives of the mentioned temperature T_{fruit}, with respect to the model parameter X_i, following the work of Aregawi et al. (2013). The relative sensitivity of the average temperature is, hence, evaluated by:

$$S_{T_{P_4},X_i} = \frac{\partial T_{fruit}/T_{fruit}}{\partial X_i/X_i} \cong \frac{T_{X_i+\Delta X_i} - T_{X_i-\Delta X_i}}{2\Delta X_i} \frac{X_i}{T} \tag{17}$$

where ΔX_i is equal to a 10% deviation from the nominal average value of X_i, in this case. The results are presented in Section 3.2.

3. Results and discussion

3.1. *Impact of airflow on fruit temperature and sensitivity analysis*

To appraise the importance of modeling the airflow around the fruit, two different models are compared. The first configuration solved for the air domain around the fruit. As such, a conjugate heat transfer is established, resulting in a local distribution of the CHTC at the fruit surface. The second model did not solve for the fluid domain, and an averaged CHTC is imposed over the solid surface. In this second model, the CHTC is evaluated from the Nusselt number presented in Eq. (16). Local distribution of the CHTC allows a more accurate representation of the heat transfer at the surface, for example between leading and trailing edges of the fruit (Fig. 4b) while an imposed averaged CHTC is not able to capture such differences. In Fig. 4a, the local distribution of the CHTC over the fruit surface is compared with the averaged values at 0.1, 1 and 10 m/s. From the graph, the impact of different velocities on the convective heat transfer coefficient distribution over the fruit surface is evident: with an increase of two orders of magnitude in the air speed, the CHTC increases by a factor of 5. Hence, not including the airflow in the model causes the loss of valuable information on the cooling heterogeneities at the surface of the product, with possible repercussions on its quality prediction.

Moreover, the importance of modeling a realistic shape is demonstrated by comparing a sphere and an ellipsoid with the

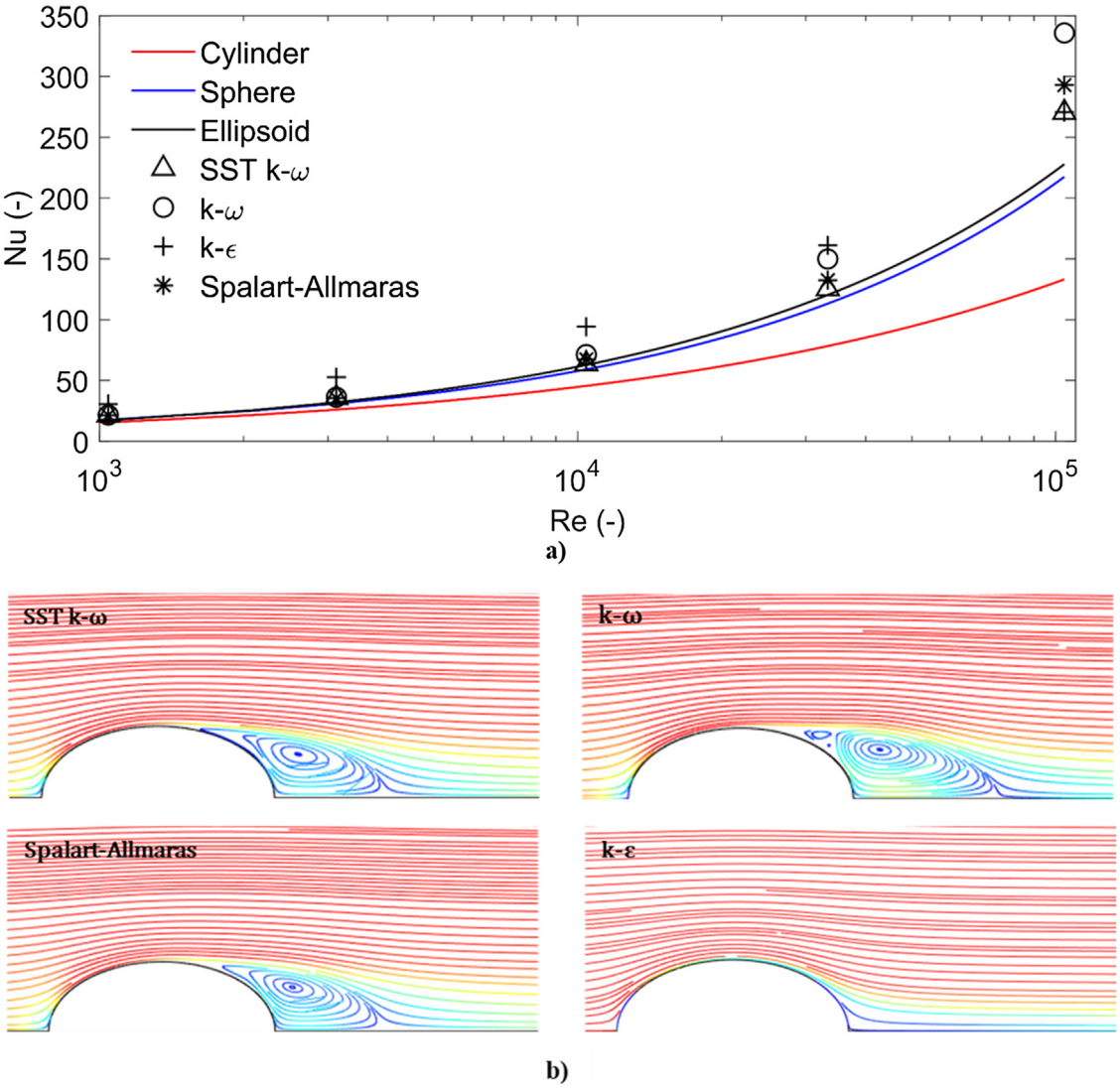

Fig. 3 – (a) Comparison of Nusselt (*Nu*) number for different turbulence models: *k–ω* shear stress transport (SST) model, *k–ω*, *k–ε* and Spalart–Allmaras, and analytical values for a sphere, a cylinder and an ellipsoid (Clary and Nelson, 1970), as a function of Reynolds number (*Re*, logarithmic scale). (b) Streamlines around an ellipsoid (side view) for different turbulence models at U_{in} = 1 m/s.

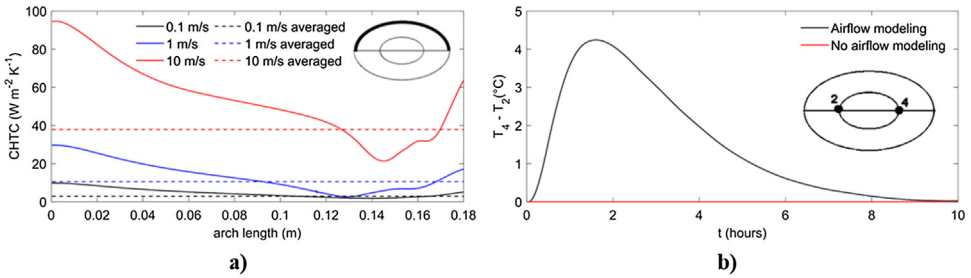

Fig. 4 – Comparison between two model configurations (at T_{in} = 10 °C), with and without the air domain. (a) From the comparison of convective heat transfer coefficients (CHTCs) evaluated at the fruit surface, it can be observed how the local distribution is suppressed with the averaged values, resulting in not capturing the temperature spatial differences. This can be also seen in (b), where the temperature difference between two different points (2 and 4) is evaluated for the two different models (with and without airflow, at the same initial conditions: T_{in} = 10 °C and U_{in} = 1 m/s).

same volume, under the same flow conditions, and evaluating the spatial distribution of the temperature. The impact on the fluid flow of the two different shapes results in a diverse local distribution of the CHTC, which directly influences the temperature distribution inside the objects, as portrayed in Fig. 5. The maximum temperature difference between two points (2 and 4) on the seed surface is 2.1 °C for the sphere and 4.2 °C inside the ellipsoid, resulting in a difference of more than 2 °C, which could negatively affect the accuracy of the fruit quality prediction. With this in mind, a realistic model that includes airflow and a realistic fruit shape is required to correctly capture the fruit temperature.

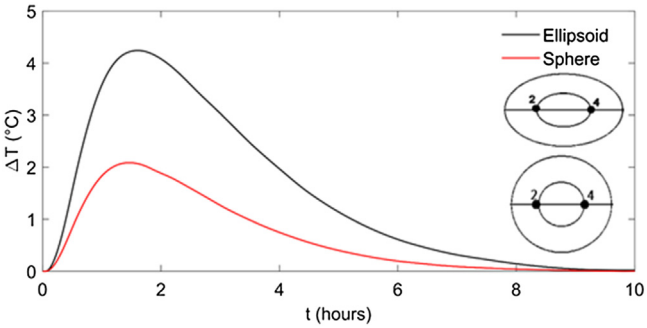

Fig. 5 – Temperature difference between points 2 and 4, for a sphere (red curve) and an ellipsoid (black curve) at T_{in} = 10 °C and U_{in} = 1 m/s. (For interpretation of the references to color in this figure legend, the reader is referred to the web version of this article.)

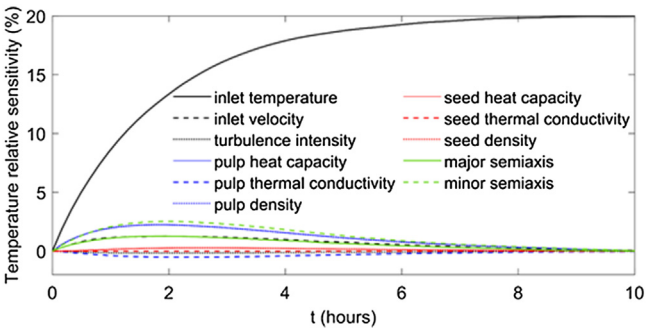

Fig. 6 – Relative sensitivity evaluated for the mean fruit temperature as a function of time for a variation of 10% of the selected input parameters.

3.2. *Sensitivity analysis*

The relative sensitivities (refer to Section 2.5) are depicted in Fig. 6 for each of the tested parameters. All the other parameters, except air temperature, produce a variation of less than 5% in the average fruit temperature for a deviation of ±10% from their initial value. The largest variation is to be found for air temperature: for a deviation of ±10% we see a variation in fruit temperature of 20%, which confirms air temperature as the most influential parameter, followed by thermal properties and fruit size.

3.3. *Temperature heterogeneities inside the fruit*

As stated in Section 1, one of the main complications during experiments is to know where the highest temperatures are inside the fruit, so that experimental temperature probes can be placed in the right positions. Since the core temperature of the mango seed is not accessible, these zones are located close to the seed, as shown in Fig. 7. In the graph, points 4 and 6 exhibit the highest temperatures and so these are the most conservative positions for temperature sensors. This simple but important estimation is possible, due to an accurate model that included not only the fluid domain but, also, the different materials (pulp and seed) that compose the fruit (see Table 1).

Although air velocity is not the most influential parameter for fruit temperature (see Section 3.2), its impact on temperature profiles and cooling uniformity cannot be ignored, since it influences the consistency of the quality attributes, and it must be achieved to avoid a rapid quality decay of some parts, with the subsequent spoilage of the commodity. Therefore,

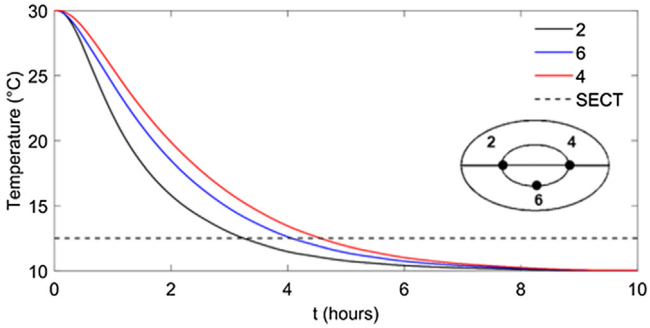

Fig. 7 – Comparison of temperatures at different inner points of the mango (2, 4 and 6), at U_{in} = 1 m/s and T_{in} = 10 °C). The 7/8 cooling time (SECT) is also shown as a dashed line to indicate the differences between the points.

along with the identification of the warmest zones within the mango, the cooling uniformity is investigated. A higher uniformity in temperatures can be attained by choosing the correct air speed. To this end, a set of simulations is carried out to examine the cooling of the mango at different air velocities. A comparison between different velocities is presented in Fig. 8a. The cooling rate is taken as the reference for the comparison and leads to the fractional unaccomplished temperature difference Y (Teruel et al., 2004), where T_{air}, T_p and T are the air temperature, the average initial fruit temperature and the actual temperature at time of observation, respectively:

$$Y = \frac{T - T_{air}}{T_p - T_{air}} \tag{18}$$

Fig. 8a can be interpreted as a comparison between temperature profiles (represented by Y) at different air speeds. By looking at the 7/8 cooling time (i.e. time required to reduce the temperature difference between the product and the refrigerating air by 7/8), it can be seen that $Y_{7/8}$ = 0.125 is reached in 1.4 h at 10 m/s, in 3.6 h at 1 m/s and, finally, in 10.3 h at 0.1 m/s.

Although a higher speed is preferable because it implies a faster cooling, it can be the cause of pronounced cooling heterogeneities. In this regard, Fig. 8b shows the difference between the maximum and the minimum fruit temperature within the fruit at three different speeds among those investigated, namely, 0.1, 1 and 10 m/s. The difference between T_{max} and T_{min} is chosen as an indicator of temperature peaks inside the fruit. Although at 10 m/s there is a peak temperature that drastically reduces with time, for 0.1 m/s the temperature difference decreases much slower, granting a better uniformity in cooling.

3.4. *Prediction of different quality attributes over time under different cooling conditions*

The last part of this work examines the evolution of different quality attributes over time and their spatial distribution inside the fruit. Besides the overall quality, this study also considered other fundamentals, such as the fruit attributes, commonly accepted as quality indicators (Dea et al., 2010; Emongor, 2015).

In Fig. 9, overall quality, firmness, total soluble solids, titratable acid, vitamin C and β-carotene are depicted as a function of time. After storage for 4 days, a considerable decrease in overall quality (first-order reaction) is seen for all storage temperatures (Fig. 9a). At 5 °C, the overall quality is at 58%, while

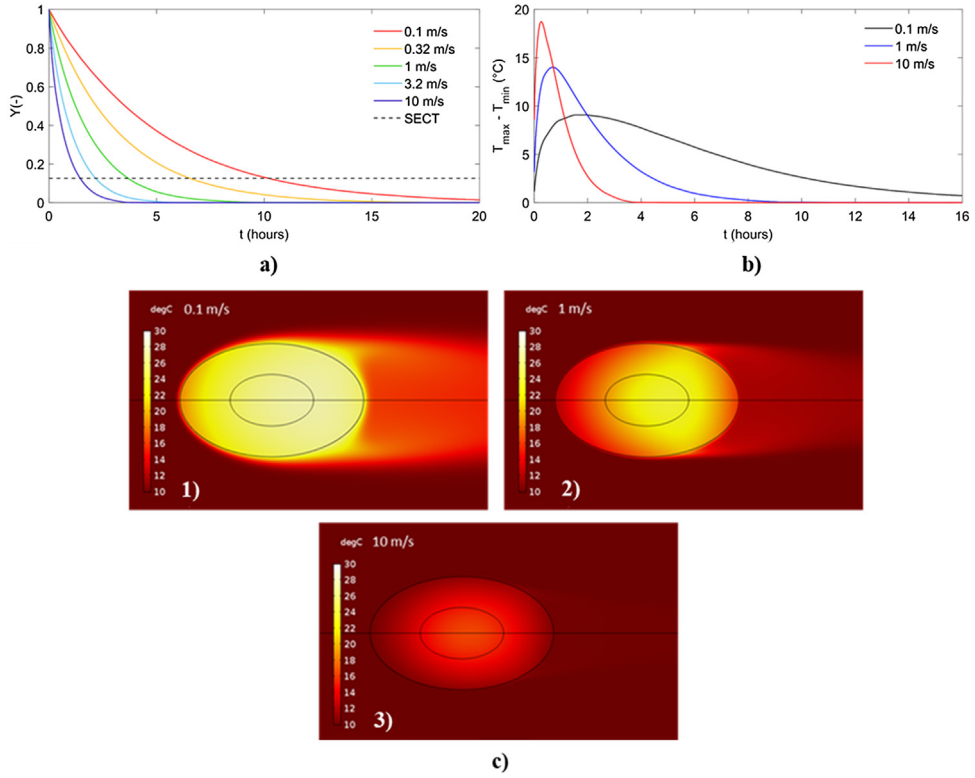

Fig. 8 – (a) Temperature profiles expressed by the fractional unaccomplished temperature difference Y (Eq. (12)) at T_{in} = 10 °C for different air speeds (U_{in}). The 7/8 cooling time is also shown to aid the comparison. (b) Temperature difference between maximum and minimum fruit temperature within the fruit at different air speeds for T_{in} = 10 °C, which shows how the best cooling uniformity can be achieved. (c) Temperature distribution within the fruit at (1) U_{in} = 0.1 m/s, (2) U_{in} = 1 m/s, and (3) U_{in} = 10 m/s, at 1 h, at T_{in} = 10 °C.

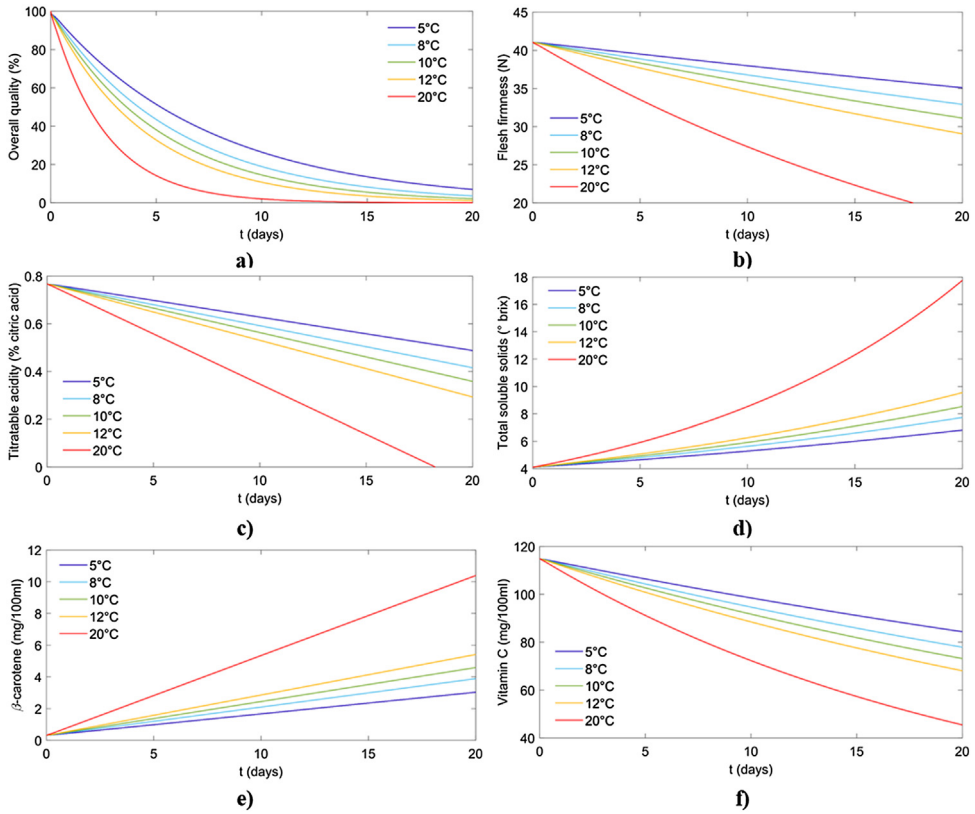

Fig. 9 – Comparison different quality attributes evolution in 20 days storage simulations at different temperatures (5, 8, 10, 12 and 20 °C). The evaluated attributes (at U_{in} = 1 m/s) are (a) overall quality, (b) flesh firmness, (c) titratable acidity, (d) total soluble solids, (e) β-carotene and (f) vitamin C.

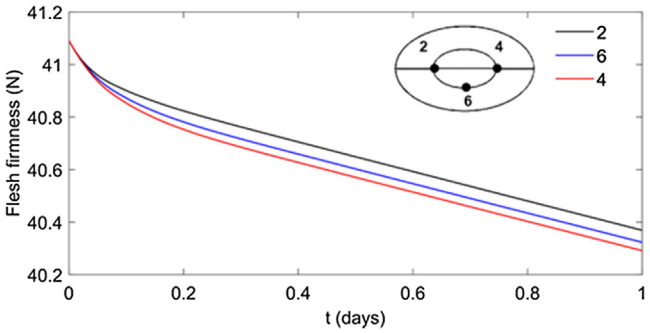

Fig. 10 – Comparison at T_{in} = 10 °C and U_{in} = 1 m/s between flesh firmness at different locations inside the fruit. The difference within a single fruit is around 0.1 N between 2 and 4 on day 1.

at 10 °C decreases further to 46%. For storage at 20 °C, less than 20% of the overall quality remains after 4 days. Hence, at 20 °C, the product will probably be spoiled at that point, but if it is kept at lower temperatures, the overall quality, and so shelf life, can be extended. The same trend is observed, for instance, in the citric acid content (zero-order reaction, Fig. 9c): at 14 days, the acidity has dropped down below 0.2% at 20 °C, already exceeding the acceptable levels for acidity, while at 8 and 12 °C, the citric acid content is still at 0.52% and 0.43%, respectively. Hence, together, the subplots in Fig. 9 demonstrate how these parameters are strongly related to temperature and how temperature regulation is of primary importance to delay fruit degradation.

The spatial heterogeneities of each quality parameter within the fruit are also investigated. As an example, flesh firmness differences among the points 2, 4 and 6 are presented in Fig. 10. Even if the difference at day 1 is almost 0.1 N and, thus, not very significant in a single fruit, it could become much larger when considering larger assemblies, like a pallet.

4. Conclusions

This study aimed to improve the understanding of the cooling behavior of a single mango fruit, a complex-shaped fruit composed of different materials, and provided an insight into the evolution of its different quality attributes under different cooling conditions.

A sensitivity analysis on the main input parameters (inlet temperature, pulp thermal properties, seed thermal properties, major and minor semi-axes, inlet velocity, turbulence intensity) showed that air temperature is the most influential parameter and, also, that a variation in 10% on the thermal properties has an impact of less than 5% on the resulting fruit temperature.

The temperature distribution within a single mango was investigated for different airspeeds at different storage temperatures, and revealed that the fruit cools down faster at high speeds. Furthermore, the cooling uniformity was evaluated as the maximum and minimum average temperature difference within the fruit at different air speeds. It demonstrated that at low speeds, a more uniform cooling can be achieved and thereby a more homogeneous quality decay within the mango, although the overall quality decay will still be faster than for high-airspeed cooling. By evaluating the heterogeneity of the temperature field, it was possible to identify the zones with the highest temperature inside the product, which can be valuable information for the placement of temperature probes.

As a result of the implementation of kinetic rate laws that describe different biochemical processes within the fruit, we identified how different fruit quality attributes (flesh firmness, titratable acidity, soluble solid content, vitamin content and β-carotene) change over time.

The model presented in this work is a reliable tool that allows the prediction of different quality attributes of a single fruit in cold chains, starting from the air temperature history. It can also be a valuable tool to prevent fruit spoilage. Specifically, it reproduces the fruit temperature history along a cold chain and, with that information, predicts the evolution of different quality attributes over time.

Acknowledgment

This work was supported by the Swiss National Science Foundation SNSF (project 200021-169372).

References

Alvarez, G., Flick, D., 1999a. Analysis of heterogeneous cooling of agricultural products inside bins. Part I: Aerodynamic study. J. Food Eng. 39, 227–237.

Alvarez, G., Flick, D., 1999b. Analysis of heterogeneous cooling of agricultural products inside bins. Part II: Thermal study. J. Food Eng. 39, 239–245.

Alvarez, G., Bournet, P.E., Flick, D., 2003. Two-dimensional simulation of turbulent flow and transfer through stacked spheres. Int. J. Heat Mass Transf. 46, 2459–2469.

Aregawi, W., Defraeye, T., Verboven, P., Herremans, E., Roeck, G., Nicolai, B., 2013. Modeling of coupled water transport and large deformation during dehydration of apple tissue. Food Bioprocess Technol. 6, 1963–1978.

ASHRAE, 2001. Fundamentals Handbook (SI). Chapter 6.

ASHRAE, 2006. Handbook – Refrigeration (SI). Chapter 19.

Baloch, M.K., Bibi, F., Jilani, M.S., 2011. Quality and shelf life of mango (*Mangifera indica* L.) fruit: as affected by cooling at harvest time. Scientia Horticulturae 130 (3), 642–646.

Beukema, K.J., Bruin, S., Schenk, J., 1982. Heat and mass transfer during cooling and storage of agricultural products. Chem. Eng. Sci. 37 (2), 291–298.

CBI – Ministry of Foreign Affairs, 2016. Exporting Mangoes to Europe.

Clary, B.L., Nelson, G.L., 1970. Determining convective heat transfer coefficients from ellipsoidal shapes. Am. Soc. Agric. Biol. Eng. 13 (3), 309–314.

COMSOL Multiphysics 5.3a, 2017. User's Guide.

Dea, S., Brecht, J.K., Nunes, M.C.N., Baldwin, E.A., 2010. Quality of fresh-cut "Kent" mango slices prepared from hot water or non-hot water-treated fruit. Postharvest Biol. Technol. 56 (2), 171–180.

Defraeye, T., Herremans, E., Verboven, P., Carmeliet, J., Nicolai, B., 2012. Convective heat and mass exchange at surfaces of horticultural products: a microscale CFD modelling approach. Agric. Forest Meteorol. 162–163, 71–84.

Defraeye, T., Lambrecht, R., Delele, M.A., Tsige, A.A., Opara, U.L., Cronjé, P., Verboven, P., Nicolai, B., 2014. Forced-convective cooling of citrus fruit: cooling conditions and energy consumption in relation to package design. J. Food Eng. 121, 118–127.

Defraeye, T., Lambrecht, R., Tsige, A.A., Delele, M.A., Opara, U.L., Cronjé, P., Verboven, P., Nicolai, B., 2013a. Forced-convective cooling of citrus fruit: package design. J. Food Eng. 118, 8–18.

Defraeye, T., Tagliavini, G., Wentao, W., Prawiranto, K., Schudel, S., Verboven, P., Bühlmann, A., 2019. Digital twins probe into food cooling and biochemical quality changes for reducing losses in refrigerated supply chains. Resour. Conserv. Recycl. 149, 778–794.

Defraeye, T., Verboven, P., Nicolai, B., 2013b. CFD modelling of flow and scalar exchange of spherical food products: turbulence and boundary-layer modelling. J. Food Eng. 114, 495–504.
Defraeye, T., Verboven, P., Opara, U.L., Nicolai, B., Cronjé, P., 2015. Feasibility of ambient loading of citrus fruit into refrigerated containers for cooling during marine transport. Biosyst. Eng. 134, 20–30.
Dehghannya, J., Kgadi, M., Vigenault, C., 2011. Mathematical modeling of air flow and heat transfer during forced convection cooling of produce considering various package vent areas. Food Control 22, 1393–1399.
Delele, M.A., Ngcobo, M.E.K., Opara, U.L., Meyer, C.J., 2013. Investigating the effects of table grape package components and stacking on airflow, heat and mass transfer using 3-D CFD modelling. Food Bioprocess Technol. 6 (9), 2571–2585.
Emongor, V., 2015. The effects of temperature on storage life of mango (*Mangifera indica* L.). Am. J. Exp. Agric. 5 (3), 252–261.
Franke, J., Hellsten, A., Schlünzen, H., Carissimo, B., 2007. Best practice guidelines for the CFD simulation of flow in the urban environment. In: COST Action 732: Quality Assurance and Improvement of Microscale Meteorological Models, Hamburg Germany.
Han, J.W., Zhao, C.J., Yang, X.T., Qian, J.P., Fan, B.L., 2015. Computational modeling of airflow and heat transfer in a vent box during cooling: optimal package design. Appl. Therm. Eng. 91, 883–893.
Karithi, E.M., 2016. Evaluation of the Efficacy of CoolbotTM Cold Storage Technology to Preserve Quality and Extend Shelf Life of Mango Fruits. Horticulture of the University of Nairobi – Department of Plant Science and Crop Protection.
Launder, B.E., Spalding, D.B., 1974. The numerical computation of turbulent flows. Comput. Methods Appl. Mech. Eng. 3, 269–289.
Menter, F.R., 1994. Two-equation eddy-viscosity turbulence models for engineering applications. AIAA J. 32 (8), 1598–1605.
Mercier, S., Villeneuve, S., Mondor, M., Uysal, I., 2017. Time–temperature management along the food cold chain: a review of recent developments. Compr. Rev. Food Sci. Food Safety 16 (4), 647–667.
Noiwan, D., Suppakul, P., Joomwong, A., Uthaibutra, J., Rachtanapun, P., 2017. Kinetics of mango fruits (*Mangifera indica* cv. "Nam Dok Mai Si Thong"). Quality changes during storage at various temperatures. J. Agric. Sci. 9 (6), 199.
Nunes, M.C.N., Emond, J.P., Brecht, J.K., Dea, S., Proloux, E., 2006. Quality curves for mango fruit (cv. Tommy Atkins and Palmer) stored at chilling and non-chilling temperatures. pdf. J. Food Qual. 30, 104–120.
Nzikou, J.M., Kimbonguila, A., Matos, L., Loumouamou, B., Pambou-Tobi, N.P.G., Ndangui, C.B., Abena, A.A., Silou, Th., Scher, J., Desobry, S., 2010. Extraction and characteristics of seed kernel oil from mango (*Mangifera indica*). Res. J. Environ. Earth Sci. 2 (1), 31–35.
O'Sullivan, J., Ferrua, M.J., Love, R., Verboven, P., Nicolaï, B., East, A., 2016. Modelling the forced-air cooling mechanisms and performance of polylined horticultural produce. Postharvest Biol. Technol. 120, 23–35.
Raval, A.H., Solanki, S.C., Yadav, R., 2013. A simplified heat transfer model for predicting temperature change inside food package kept in cold room. J. Food Sci. Technol. 50 (2), 257–265.
Redding, G.P., Yang, A., Shim, Y.M., Olatunji, J., East, A., 2016. A review of the use and design of produce simulators for horticultural force-air cooling studies. J. Food Eng. 190, 80–93.
Roache, P.J., 1994. Perspective: a method for uniform reporting of grid refinement studies. J. Fluids Eng. 116 (3), 405.
Robertson, G.L., 1993. Food Packaging: Principles and Practices. Marcel Dekker, Inc.
Saudreau, M., Sinoquet, H., Santin, O., Marquier, A., Adam, B., 2007. A 3D model for simulating the spatial and temporal distribution of temperature within ellipsoidal fruit. Agric. Forest Meteorol. 147 (1–2), 1–15.
Spalart, P.R., Allmaras, S.R., 1992. A one-equation turbulence model for aerodynamic flows. AIAA Paper, 92–439.
Teruel, B., Kieckbusch, T., Cortez, L., 2004. Cooling parameters for fruits and vegetable of different sizes in a hydrocooling system. Scientia Agricola 61 (6), 655–658.
Van Boekel, M.A.J.S., 2008. Kinetic modeling of food quality: a critical review. Compr. Rev. Food Sci. Food Safety 7, 144–158.
Wilcox, D.C., 1988. Re-assessment of the scale-determining equation for advanced turbulence models. AIAA J. 26 (11), 1299–1310.
Wu, W., Defraeye, T., 2018. Identifying heterogeneities in cooling and quality evolution for a pallet of packed fresh fruit by using virtual cold chains. Appl. Therm. Eng. 133, 407–417.
Zhao, C.J., Han, J.W., Yang, X.T., Qian, J.P., Fan, B.L., 2016. A review of computational fluid dynamics for forced-air cooling process. Appl. Energy 168, 314–331.
Zou, Q., Opara, L.U., McKibbin, R., 2006. A CFD modeling system for airflow and heat transfer in ventilated packaging for fresh foods: I. Initial analysis and development of mathematical models. J. Food Eng. 77 (4), 1037–1047.